Microchimica Acta (2022) 189: 24
https://doi.org/10.1007/s00604-021-05128-x

ORIGINAL PAPER

A molecularly imprinted electrochemical biosensor based on hierarchical $Ti_2Nb_{10}O_{29}$ (TNO) for glucose detection

Ceren Karaman[1] · Onur Karaman[2] · Necip Atar[3] · Mehmet Lütfi Yola[4]

Received: 24 August 2021 / Accepted: 2 December 2021 / Published online: 11 December 2021

Abstract

A novel molecularly imprinted electrochemical biosensor for glucose detection is reported based on a hierarchical N-rich carbon conductive-coated TNO structure (TNO@NC). Firstly, TNO@NC was fabricated by a novel polypyrrole-chemical vapor deposition (PPy-CVD) method with minimal waste generation. Afterward, the electrode modification with TNO@NC was performed by dropping TNO@NC particles on glassy carbon electrode surfaces by infrared heat lamp. Finally, the glucose-imprinted electrochemical biosensor was developed in presence of 75.0 mM pyrrole and 25.0 mM glucose in a potential range from + 0.20 to + 1.20 V versus Ag/AgCl via cyclic voltammetry (CV). The physicochemical and electrochemical characterizations of the fabricated molecularly imprinted biosensor was conducted by transmission electron microscopy (TEM), scanning electron microscopy (SEM), X-ray diffraction (XRD) method, X-ray photoelectron spectroscopy (XPS), electrochemical impedance spectroscopy (EIS), and CV techniques. The findings demonstrated that selective, sensitive, and stable electrochemical signals were proportional to different glucose concentrations, and the sensitivity of molecularly imprinted electrochemical biosensor for glucose detection was estimated to be 18.93 μA μM^{-1} cm^{-2} ($R^2 = 0.99$) at + 0.30 V with the limit of detection (LOD) of 1.0×10^{-6} M. Hence, it can be speculated that the fabricated glucose-imprinted biosensor may be used in a multitude of areas, including public health and food quality.

Keywords Glucose biosensor · Molecularly imprinting · Electrochemistry · $Ti_2Nb_{10}O_{29}$

Introduction

Chronic diabetes disease has been affecting a large number of people all around the world, thereby developing a non-invasive glucose detection technique with high sensitivity, and low cost is of substantial importance [1, 2]. Several methods, such as colorimetry [3], gas or liquid chromatography [2, 4], fluorescence [5], Fourier transform infrared spectroscopy [6], chem- or electrochemiluminescence [7, 8], and electrochemical techniques [9], have been employed to determine the glucose level in human serum and foodstuffs during the last few decades. However, there are some shortcomings of glucose determination by reported methods. Specifically, various other substances in the environment during glucose measurement, such as acetaminophen, uric acid, and ascorbic acid, may interact with glucose; thus, a high amount of samples is necessary for glucose determination [9]. Hence, the advantages of the simpler and less expensive techniques might be considerable in terms of therapeutic benefit. In this respect, electrochemical sensors appear to be one of the most promising approaches to detect glucose with high sensitivity, ease of use, and cheap cost.

Electrochemical sensors have risen to prominence among many other analytical techniques because of their simplicity of use, versatility, and low cost. Although enzyme-based electrochemical glucose sensors have been widely used to date, their high cost, sensitivity to operation conditions (such as pH and temperature), and intrinsic instability of natural enzymes restrict their further applicability [10]. As a result, enzyme-free glucose

✉ Mehmet Lütfi Yola
mlutfi.yola@hku.edu.tr

1 Department of Electricity and Energy, Vocational School of Technical Sciences, Akdeniz University, Antalya, Turkey

2 Department of Medical Imaging Techniques, Vocational School of Health Services, Akdeniz University, Antalya, Turkey

3 Department of Chemical Engineering, Faculty of Engineering, Pamukkale University, Denizli, Turkey

4 Department of Nutrition and Dietetics, Faculty of Health Sciences, Hasan Kalyoncu University, Gaziantep, Turkey

sensors have attracted substantial attention in the nanotechnology field, thanks to their several advantages such as long-term stability, ease of operation, cost-effectiveness, and portability [10, 11]. For instance, the perovskite-based electrochemical biosensors for glucose detection have been currently presented in literature [12]. The perovskites formulated as ABO_3 (A, alkali metal or a lanthanide; B, transition metal; and O, oxygen ion) demonstrate good electrocatalytic effect against bioactive molecules such as glucose and dopamine [13–15].

Along with all the aforementioned aspects in mind, nanomaterials have been regarded as a viable option for preventing drawbacks and enhancing electrode performance due to their exceptional physicochemical characteristics. $Ti_xNb_yO_z$ materials with nanosize such as $TiNb_{24}O_{62}$ [16], $Ti_2Nb_{10}O_{29}$ [17], and $TiNb_2O_6$ [18] have been currently used for electrochemical sensor application or energy storage. Especially, $Ti_2Nb_{10}O_{29}$ is very important in terms of its high theoretical capacities of about 400 mAh g^{-1}, providing efficient coating for the preparation of novel composites [19]. $Ti_xNb_yO_z$ materials' crystal structure is similar to H-Nb_2O_5 family with about 3 octahedral long in length and width [20]. In crystal structure, Ti^{4+} selectively stayed on edge sites of the blocks, providing ionic conductivity [21]. The limited electrical conductivity of $Ti_xNb_yO_z$ materials also can be improved by carbon coating [22] and nanostructuring [23]. The production of $Ti_xNb_yO_z$ materials can be performed by solid-state synthesis until 1000 °C providing particles having the size of 10–60 µm [24]. In addition, PPy-CVD method was utilized for preparation of carbon conductive-coated TNO structure (TNO@NC). Thus, TNO@NC provides the improved electrical conductivity and volumetric capacity [25].

The molecular imprinting technique has been employed to prepare polymers with selective recognition sites for the target molecules [26]. Thanks to their high affinity and selectivity, comparable to natural receptors, enhanced stability comparing to biomolecules, ease of manufacture, and adaptability to a variety of practical applications, molecularly imprinted polymers have gained considerable prominence [27]. Furthermore, molecularly imprinted polymers are favored owing to their superior mechanical characteristics, heat and pressure tolerance, physical endurance, and chemical stability in acids, bases, metal ions, and organic solvents. Thanks to these characteristics, molecularly imprinted polymers might well be utilized for identification and separation objectives in a variety of disciplines, including life, pharmaceutical, and environmental sciences [28]. These polymers' high stability, low cost, and the polymerization steps in harmony with micro-production used in sensor technology allow it to be used as a synthetic recognition element in many practical applications [29]. Therefore, molecularly imprinted polymers are increasingly being utilized in the fabrication of biosensors and nanosensors [30].

Herein, in the light of all aforementioned points in mind, it was aimed to fabricate a novel molecularly imprinted electrochemical biosensor-based N-rich carbon conductive-coated TNO structure for glucose detection for the first time in literature. The developed biosensor provided a number of advantages including ease of application, fast, and high selectivity. In addition, a sensitive LOD of 1.0×10^{-6} M was obtained, and glucose detection was performed with high selectivity without interference in plasma samples. Hence, the fabricated enzyme-free glucose sensor based on molecularly imprinted polymer paves the way for a new perspective in the monitoring glucose level in plasma samples.

Experimental section

Materials

D-glucose (D-GLU), ascorbic acid (AA), uric acid (UA), bovine serum albumin (BSA), sodium chloride (NaCl), pyrrole, niobium (V) oxide (Nb_2O_5, 99.99%), Fe (III) p-toluenesulfonate, pyrrole (98%), metatitanic acid ($TiO(OH)_2$), and anatase TiO_2 were purchased from Sigma-Aldrich. As a supporting electrolyte and dilution buffer, 0.1 M phosphate-buffered saline (PBS) solution (pH 7.0) was employed.

Apparatus for characterization of nanomaterials

Surface morphological characteristics were explored by using both a ZEISS EVO 50 SEM and a JEOL 2100 TEM. X-ray patterns of nanomaterials was recorded by a Rigaku X-ray diffractometer with Cu-K radiation ($\lambda = 0.150$ nm). The PHI 5000 Versa Probe spectrometer was used to perform the XPS survey. Electrochemical characterization techniques such as CV, EIS, and differential pulse voltammetry (DPV) were also conducted using the Gamry Reference 600 workstation (Gamry, USA).

TNO@NC synthesis

TNO@NC was synthesized using a solid-state reaction method assisted by PPy-CVD. In this technique, Nb_2O_5 (10.0 g) was billed in ultra-quality water at 1000 rpm over 2 h. Subsequently, the material was dispersed in Fe (III) p-toluenesulfonate solution (30.0 wt%) to provide the covering of Nb_2O_5 with Fe^{3+} ions ($Nb_2O_5@Fe^{3+}$), which ensured the pyrrole polymerization on $Nb_2O_5@Fe^{3+}$ surface [31]. Subsequently, pyrrole vapor (2.0 mL) was introduced into $Nb_2O_5@Fe^{3+}$ mixture at 25 °C to provide the pyrrole polymerization resulting in polypyrrole (PPy). After 60 min, the powder was washed with methanol several times to eliminate Fe^{3+} ions and residual pyrrole monomers. The obtained product was tagged as $Nb_2O_5@PPy$. After that, Nb_2O_5@PPy

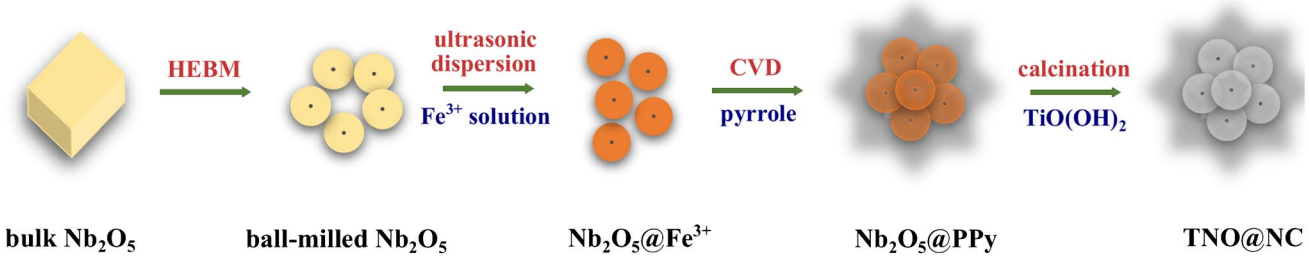

Scheme 1 Schematic preparation procedure for TNO@NC sample

was ground with $TiO(OH)_2$ for 90 min before being calcined at 500 to 900 °C for 24 h in a high-purity N_2 atmosphere (*TNO@NC*). Meanwhile, as a control experiment, *TNO* was similarly fabricated via solid-state reaction of Nb_2O_5 powder and anatase TiO_2. Scheme 1 illustrated the schematic representation of the preparation procedure for the final product TNO@NC.

Preparation of electrode

The glassy carbon electrode (GCE) was prepared as follows to be utilized in the further steps [32]: Firstly, 0.1 µm and 0.05 µm alumina slurries were transferred on cleaning pads, respectively. Following, the GCE was polished with these alumina slurries for 20 min. Then, the electrodes were rinsed with isopropyl alcohol and acetonitrile, respectively, to remove the alumina remains at 25 °C.

The electrode modifications with Nb_2O_5@PPy, TNO, and TNO@NC suspensions (20.0 µL, 0.2 mg mL^{-1}) were performed by dropping these suspensions on the clean GCEs. After 30 min, the solvent removal was carried out by infrared heat lamp, providing Nb_2O_5@PPy, TNO, and TNO@NC-modified GCEs (*Nb_2O_5@PPy/GCE*, *TNO/GCE*, and *TNO@NC/GCE*).

Preparation of D-GLU-imprinted sensor and D-GLU removal from electrode surface

In the presence of 75.0 mM pyrrole solution (as a monomer) containing 25.0 mM D-GLU (as a target molecule) in 0.1 M PBS (pH 7.0), each of the D-GLU-imprinted GCEs were constructed via 20 subsequent CV cycles at a potential scan rate of 200 mV s^{-1} and a potential range of + 0.20 to + 1.20 V. Each of the D-GLU-imprinted GCEs were tagged as *MIP/bare GCE*, *MIP/Nb_2O_5@PPy/GCE*, *MIP/TNO/GCE*, and *MIP/TNO@NC/GCE*, separately. Ag/AgCl(aq) and Pt wire were utilized as the reference and the counter electrodes, respectively. In addition, to confirm the high imprinting selectivity, D-GLU non-imprinted TNO@NC/GCE (*NIP/TNO@NC/GCE*) was prepared in the presence 75.0 mM pyrrole solution as monomer in 0.1 M PBS (pH 7.0) without analyte molecule.

To remove the target molecules (D-GLU) on electrode surface, the prepared imprinted electrodes were immersed into 2.0 M NaCl as desorption agent to eliminate the interactions between polar groups of pyrrole and D-GLU molecules. This treatment approach was continued for 20 min as elution time at 150 rpm. Finally, the electrodes such as MIP/bare GCE, MIP/Nb_2O_5@PPy/GCE, MIP/TNO/GCE, and MIP/TNO@NC/GCE were dried with nitrogen gas at 25 °C.

Sample preparation

On Supplementary Data, the sample preparation process was detailed [33].

Results and discussion

Characterization studies

According to Fig. 1A and B, high-energy ball milling (HEBM) treatment provided the reduction of the particle size of Nb_2O_5 from micron to 30 to 35 nm. Then, Nb_2O_5 nanoparticles were dispersed in Fe (III) p-toluenesulfonate solution for covering of Nb_2O_5 nanoparticles with a layer of oxidant. The chemical polymerization of pyrrole was initiated by $Nb_2O_5@Fe^{3+}$. $Nb_2O_5@Fe^{3+}$ was transferred into a tube including pyrrole vapor to form polypyrrole (PPy) on $Nb_2O_5@Fe^{3+}$ surface. The agglomeration of Nb_2O_5 nanoparticles with larger dimensions (250–350 nm) simultaneously occurred (Fig. 1C). This increased particle size is beneficial in terms of the electrochemical activity enhancement of the material [34]. According to Fig. 1D, the particle sizes were observed about 35–38 nm, while the thickness of the carbon layer was detected in a range between 1 and 5 nm (Fig. 1E). The d-spacing values of 0.349 and 0.267 nm are harmony with (400) and (215) planes for monoclinic TNO, respectively (Fig. 1E). PPy coating ensured to inhibit the sintering

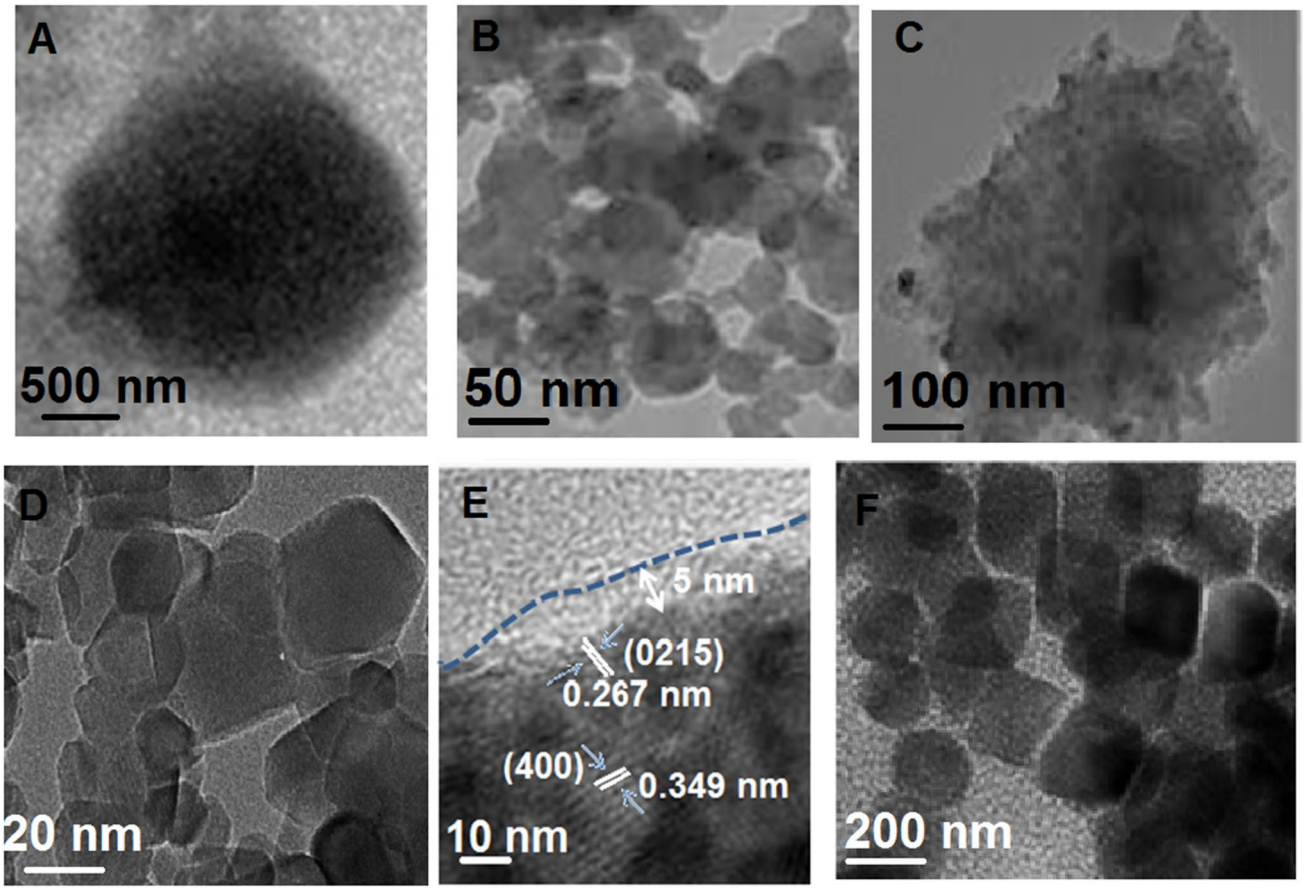

Fig. 1 TEM images of **A** bulk Nb_2O_5, **B** ball-milled Nb_2O_5, **C** Nb_2O_5@PPy, **D** TNO@NC, **E** HRTEM image of TNO@NC, and **F** TEM image of pristine TNO

of TNO as seen on Fig. 1D and F showing different particle size between TNO@NC and TNO.

The phase investigations of the product TNO@NC at calcination temperatures between 500 and 900 °C for 24 h were carried out by XRD (Fig. 2). According to Fig. 2, the phase structure of 500-TNO@NC looked alike bronze structure such as T-Nb_2O_5 [20]. For 600-TNO@NC product, the formation of the monoclinic-TNO phase was observed. Then, the bronze structure disappeared with novel weak peaks at 23.1° and 26.5° for 700-TNO@NC product in harmony with pure monoclinic TNO [35]. The monoclinic phase was formed for 800-TNO@NC and 900-TNO@NC products with higher peak intensity, demonstrating the high crystallinity of the oxide with temperature. SEM images of TNO@NC products were also observed (Fig. S1) for investigating the morphological properties. The secondary particle size of 700-TNO@NC was similar to that of 500-TNO@NC and 600-TNO@NC products owing to the effect of the carbon layer on particle growth. The particle size of 800-TNO@NC was slightly larger than that of 700-TNO@NC. When the morphology of 900-TNO@NC was investigated, the particle size increased, demonstrating the disappearance of carbon layer effect on particle growth. Fig. S2 confirmed the presence of an amount of nitrogen and the homogenous coating. Hence, it could be mentioned that nitrogen doping treatment increases electron transfer kinetics [36, 37].

High-resolution XPS spectra of N1s, C1s, Ti2p, Nb3d, and O1s of TNO@NC was presented on Fig. S3. The conversions of Ti^{4+} and Nb^{5+} into Ti^{3+} and Nb^{4+} on TNO@NC were observed (Fig. S3A and B) [38, 39]. This conversion verified TNO@NC formation in comparison with pristine TNO. In addition, N1s and C1s XPS spectra (Fig. S3D and E) showed Ti-N chemical bond formation [36], indicating high electronic conductivity of Ti-N. According to O1s spectra (Fig. S3C), the peak at 529.5 eV shifted higher binding energy for TNO@NC product in comparison with pristine TNO, demonstrating electron drain in the oxide matrix [40]. This situation showed the oxygen deficient in lattice [41]. In addition, ratio analysis of the peaks in XPS spectrum of pristine TNO and TNO@NC was evaluated (Table S1).

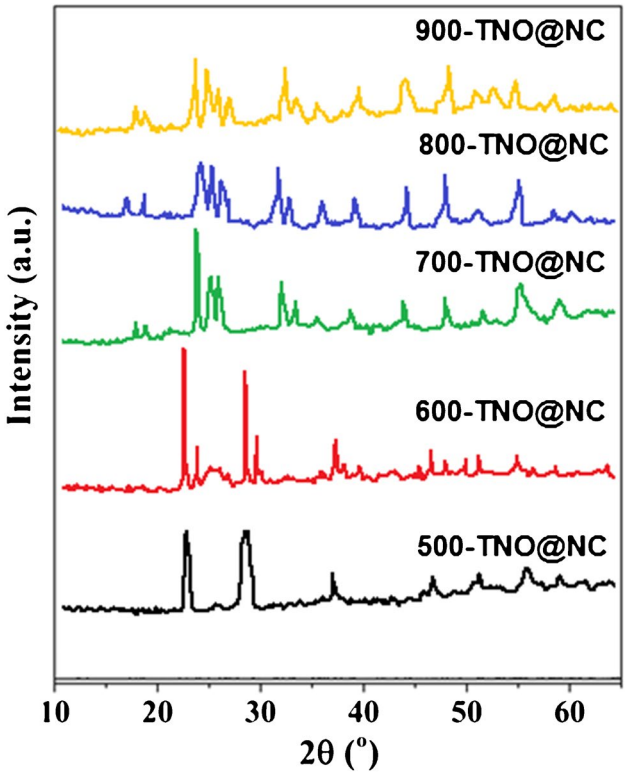

Fig. 2 XRD pattern of TNO@NC products at different calcination temperatures between 500 and 900 °C for 24 h

CV and EIS characterizations of Nb_2O_5@PPy, TNO@NC, and TNO-modified electrodes

Electrochemical investigations for modified electrodes were progressively performed by using CV and EIS methods in presence of 1.0 mM $[Fe(CN)_6]^{3-/4-}$ as redox pair. Firstly, the anodic and cathodic signals on bare GCE were observed at Epa = 500 mV and Epc = 250 mV, respectively (curve a of Fig. 3A). When Nb_2O_5@PPy/GCE was used towards 1.0 mM $[Fe(CN)_6]^{3-/4-}$, the more obvious electrochemical signals were obtained in comparison with bare GCE (curve b of Fig. 3A) owing to high conducting polymer structure of PPy [42]. Then, due to TNO's high theoretical capacity (400 mAh g^{-1}) and fast electrochemical reaction kinetics, there was more electrochemical catalytic effect on the signals (curve c of Fig. 3A) [43]. Finally, the electronic conductivity, specific area and porous nano-structure of a hierarchical N-rich carbon conductive-coated TNO structure provided the highest electrochemical responses in comparison with TNO/GCE (curve d of Fig. 3A) [22, 23]. The values of peak potential difference (ΔEp) were also calculated as 250 mV for bare GCE, 200 mV for Nb_2O_5@PPy/GCE, 160 mV for TNO/GCE, and 130 mV for TNO@NC/GCE. Finally, the specific surface areas of bare GCE, Nb_2O_5@PPy/GCE, TNO/GCE, and TNO@NC/GCE were calculated as 0.170 ± 0.06 cm^2, 0.486 ± 0.03 cm^2, 0.708 ± 0.04 cm^2, and 1.193 ± 0.02 cm^2 in the presence of $[Fe(CN)_6]^{3-}$, respectively, by Randles–Sevcik equation [44]. This situation shows that TNO@NC product can be used as electrochemical sensor for sensitive determination of D-GLU.

EIS experiments were performed to prove CV results and according to Fig. 3B, the obtained charge transfer resistances were calculated as 160, 135, 110, and 90 Ω for bare GCE, Nb_2O_5@PPy/GCE, TNO/GCE, and TNO@NC/GCE, respectively. Hence, the highest electrical conductivity and the easiest electron transfer occurred on TNO@NC/GCE, indicating in coherence with CV results.

Formation of D-GLU-imprinted polymer on TNO@NC/GCE

For the formation of D-GLU-imprinted polymer on TNO@NC/GCE, 75.0 mM pyrrole solution containing 25.0 mM D-GLU was transferred into electrochemical cell. According to Fig. 4A, during the applied potential scan, the obvious oxidation peaks at about + 0.80 V were observed. Nonetheless, these polymerization peaks started to decrease after first scan and disappeared at 20th

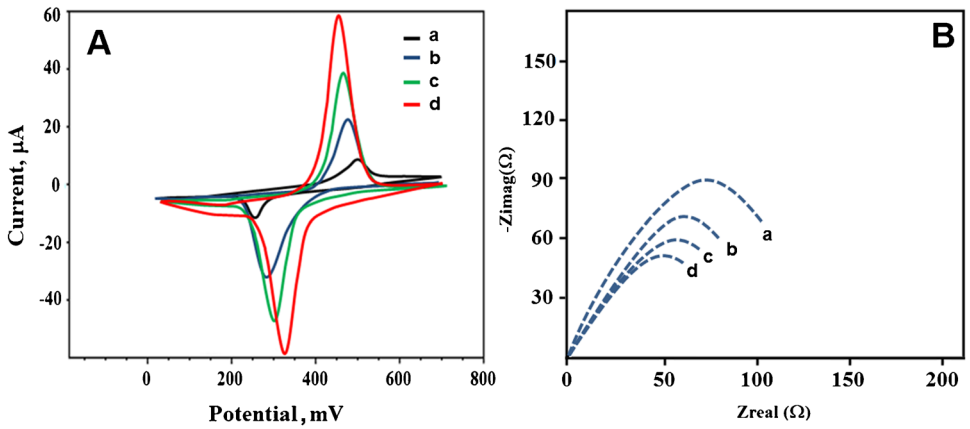

Fig. 3 **A** Cyclic voltammograms and **B** EIS responses at (a) bare GCE, (b) Nb_2O_5@PPy/GCE, (c) TNO/GCE, (d) TNO@NC/GCE, Redox probe: 1.0 mM $[Fe(CN)_6]^{3-/4-}$ containing 0.1 M KCl, scan rate: 100 mV s^{-1}

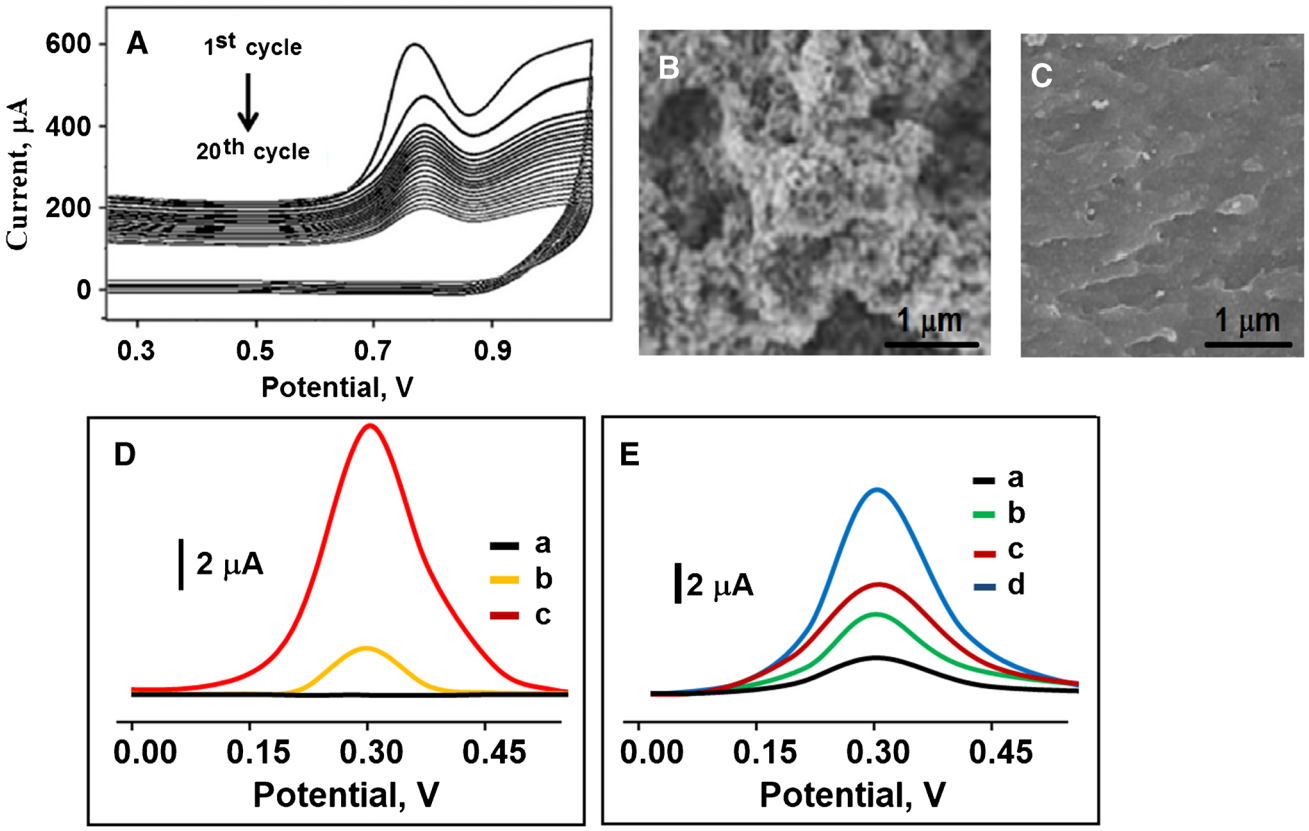

Fig. 4 **A** Polymerization of 75.0 mM pyrrole containing 25.0 mM D-GLU on TNO@NC/GCE (scan rate: 100 mV s^{-1}); SEM images of **B** MIP/TNO@NC/GCE and **C** NIP/TNO@NC/GCE, **D** differential pulse voltammograms (DPVs) of the prepared electrodes in this study: (a) MIP/TNO@NC/GCE in blank buffer solution (pH 7.0), (b) NIP/TNO@NC/GCE after rebinding of 0.500 mM D-GLU in 0.1 M PBS (pH 7.0), (c) MIP/TNO@NC/GCE after rebinding of 0.500 mM D-GLU in 0.1 M PBS (pH 7.0) (parameters are frequency of 100 Hz, pulse amplitude of 25 mV and scan increment of 5 mV); **E** DPVs of different molecularly imprinting electrodes after rebinding of 0.500 mM D-GLU in 0.1 M PBS (a) MIP/bare GCE, (b) MIP/Nb_2O_5@PPy/GCE, (c) MIP/TNO/GCE, (d) MIP/TNO@NC/GCE (parameters are frequency of 100 Hz, pulse amplitude of 25 mV, and scan increment of 5 mV)

cycle. Hence, this disappearance on the oxidation peaks confirmed the formation of D-GLU imprinted polymer on TNO@NC/GCE. The prepared MIP and NIP surfaces were investigated in terms of morphological features (Fig. 4B and C). As expected, apparent porous polymeric structures on Fig. 4B and non-porous polymeric structures on Fig. 4C were observed. Finally, in order to demonstrate the imprinting selectivity, the electrochemical properties of the prepared MIP and NIP electrodes were investigated. The electrochemical signals were not observed by MIP/TNO@NC/GCE in blank buffer solution without D-GLU (curve a of Fig. 4D). However, MIP/TNO@NC/GCE demonstrated the obvious electrochemical signals belonging to D-GLU at + 0.30 V in the presence of 0.5 mM D-GLU in 0.1 M PBS (curve c of Fig. 4D). In addition, as expected, the smaller signals were observed by NIP/TNO@NC/GCE in the presence of 0.5 mM D-GLU in 0.1 M PBS (curve b of Fig. 4D). Thus, it was confirmed that the molecular imprinting is an efficient technique providing the high selective detection in complex samples [45]. Lastly, the different molecular-imprinted electrochemical biosensors (MIP/bare GCE, MIP/Nb_2O_5@PPy/GCE, MIP/TNO/GCE, MIP/TNO@NC/GCE) were gradually prepared to show the electrochemical activity of the final biosensor. According to Fig. 4E, the highest electrochemical signal was observed by using MIP/TNO@NC/GCE (curve d of Fig. 4E) thanks to the enhancement of electron transfer ability resulting from nitrogen doping.

Optimization studies

The important parameters such as pH, mole ratio D-GLU to pyrrole monomer, desorption time, and scan cycle were investigated on Fig. S4 of Supplementary Data.

Linearity range and electrochemical mechanism

Typical glucose levels in human blood for type 2 diabetes normally vary in the range from 4.0×10^{-3} to 5.0×10^{-3} M before having a meal and should be less than 7.0×10^{-3} M within 1–2 h after a meal [46, 47]. Figure 5 showed DPVs including the observed electrochemical signals against D-GLU concentration (from 0.01 to 5.0 mM) by using MIP/TNO@NC/GCE and NIP/TNO@NC/GCE. Hence, a certain linearity for MIP and NIP biosensors was obtained as $y\ (\mu A) = 19.811x\ (mM) + 0.1927$ and $y\ (\mu A) = 7.9818x\ (mM) + 0.3735$, respectively, in this concentration range. It was concluded that the molecularly imprinting provided important advantages such as high selectivity and sensitivity towards D-GLU determination in harmony with Fig. 4D.

D-GLU's electrooxidation to glucolactone was catalyzed by MIP/TNO@NC/GCE according to the following electrochemical reaction [48]:

$$\text{Glucose} \rightarrow e^- + \text{Glucolactone} \quad (1)$$

Then, to highlight the possible electrochemical reaction mechanism, the different cyclic voltammograms (Fig. 6) curves at MIP/TNO@NC/GCE in pH 7.0 of PBS in 1.0 mM D-GLU solution at different scan rates (from 10 to 100 mV s^{-1}) and anodic/cathodic currents as a function of square root of scan rate were obtained. According to Fig. 6, the following linear regression equations were obtained below:

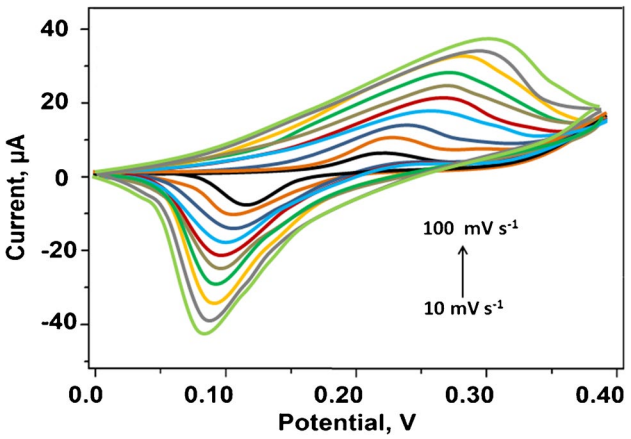

Fig. 6 Cyclic voltammograms curves at MIP/TNO@NC/GCE in pH 7.0 of PBS in 1.0 mM D-GLU solution at different scan rates (from 10 to 100 mV s^{-1})

$$\text{Ipa} = 3.8106(\text{v})^{1/2} + 5.0398(R^2 = 0.9997) \quad (2)$$

$$\text{Ipc} = -3.9317(\text{v})^{1/2} - 6.0979(R^2 = 0.9993) \quad (3)$$

A linear relationship justified a diffusion-controlled electrochemical process for the electrooxidation of D-GLU.

The sensitivity of the developed electrochemical MIP biosensor for glucose detection was determined by Eq. (4) and Eq. (5).

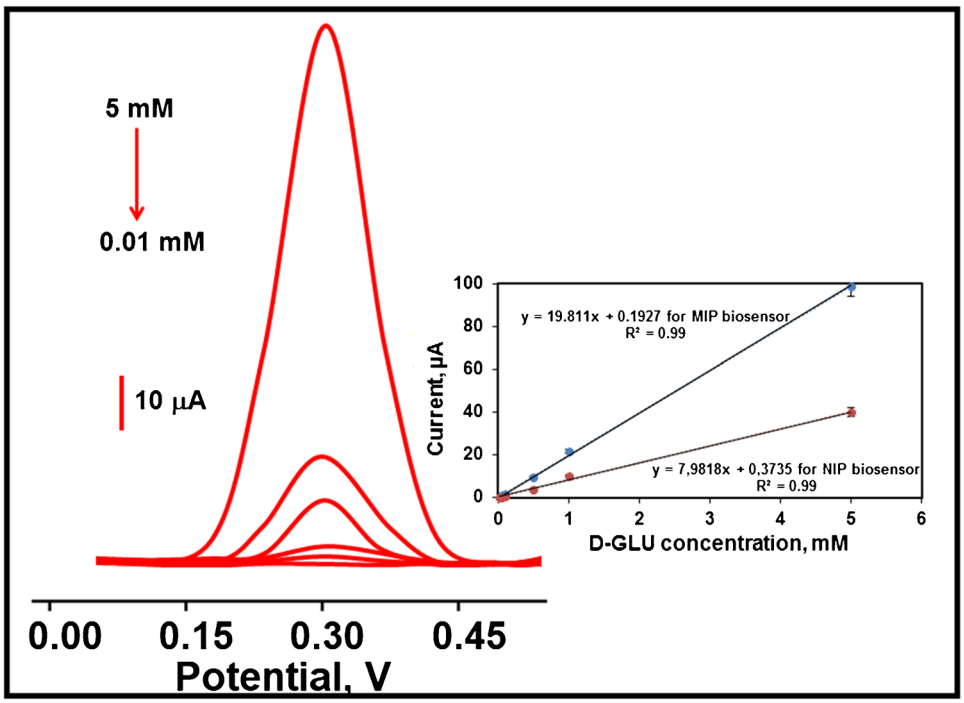

Fig. 5 Differential pulse voltammograms with different D-GLU amounts at MIP/TNO@NC/GCE in pH 7.0 of PBS (from 0.01 to 5.0 mM). Inset: D-GLU's calibration curves for MIP and NIP biosensors ($n = 6$) (parameters are frequency of 100 Hz, pulse amplitude of 25 mV, and scan increment of 5 mV)

$$LOQ = 10.0S/m \quad (4)$$

$$LOD = 3.3S/m \quad (5)$$

where S is standard deviation of intercept value on calibration equation for MIP biosensor and m is slope on calibration equation for MIP biosensor. According to Eq. (4) and Eq. (5), the values of limit of quantification (LOQ) and LOD were calculated as 1.0×10^{-5} and 1.0×10^{-6} M, respectively. Table 1 demonstrated some important comparisons such as sensitivity between D-GLU-imprinted TNO@NC/GCE and other glucose detection methods. Firstly, it was shown that glucose determination can be made in high sensitivity. Secondly, thanks to molecular imprinting technique, the glucose determination can be performed with high selectivity in complex sample such as plasma. During the preparation of N-rich carbon conductive-coated TNO structure, owing to solid-state reaction technique, an environmentally and human-friendly biosensor is achieved in terms of minimum waste generation. Finally, the portable, stable, and reproducible molecularly imprinting biosensor for glucose determination was developed in this study.

Recovery

Recovery experiments showed that glucose determination was performed with high selectivity without any interference. According to Table S2, the fabricated molecularly imprinted electrochemical biosensor was of a detection ability in complex plasma samples due to the values to approximately 100.00%. Furthermore, standard addition method was applied to the prepared plasma samples, and the calibration equation of $y\ (\mu A) = 19.197x\ (mM) + 10.0846$ was obtained by using MIP biosensor. Hence, the close slopes between direct calibration and standard addition methods confirmed the high selective glucose determination without interference.

The validity of the molecular imprinted biosensor was investigated by LC/MS [57]. Table S3 indicated the comparison results, showing that no significant difference was observed between the prepared biosensor and LC/MS ($T_{calculated} > T_{tabulated}$, $p > 0.05$).

Selectivity, stability, reusability, and reproducibility

For the selectivity test of D-GLU-imprinted electrochemical biosensor, some agents such as AA, UA, BSA, and NaCl with a high probability of co-existing with glucose in the plasma sample were preferred. As seen in Fig. 7A, the prepared D-GLU imprinted electrochemical biosensor showed the highest electrochemical affinity towards D-GLU, as expected. Likewise, the prepared D-GLU-imprinted electrochemical biosensor showed low affinity for other agents of 100.0 mM AA, 100.0 mM UA, 100.0 mM BSA, and 100.0 mM NaCl (Fig. 7A). This low affinity resulted from the physicochemical properties between D-GLU and the other agents. Secondly, to demonstrate the imprinting selectivity of D-GLU-imprinted electrochemical biosensor, D-GLU non-imprinted electrochemical biosensor (NIP/TNO@NC/GCE) was applied to 0.500 mM D-GLU, 100.0 mM AA, 100.0 mM UA, 100.0 mM BSA, and 100.0 mM NaCl, and these results were shown on Fig. 7B and Table 2. As expected, NIP/TNO@NC/GCE showed the low electrochemical affinity against D-GLU and the other agents. In addition, the calculated selectivity coefficients (k) and relative selectivity coefficients (k') values were tabulated, according to k and k' values, it can be concluded that D-GLU imprinting procedure provided the high selectivity against D-GLU analysis in complex samples.

For the stability of D-GLU-imprinted electrochemical biosensor (MIP/TNO@NC/GCE), the prepared electrode was applied to 0.500 mM D-GLU during 60 days. The

Table 1 Comparison of the proposed D-GLU electrochemical biosensor with other analytical methods

Material or method	Linear range (M)	LOD (M)	Ref
CuO/ITO electrode	1.0×10^{-5}–4.0×10^{-3}	3.0×10^{-6}	[49]
rGO/APBA	1.0×10^{-4}–1.0×10^{-3}	2.6×10^{-5}	[50]
APBA/GNPs	1.0×10^{-3}–5.0×10^{-2}	5.0×10^{-5}	[51]
CNTs/PBA	1.0×10^{-6}–1.0×10^{-4}	1.2×10^{-5}	[52]
Alkyne/boronic acid/SERS	1.0×10^{-4}–100.0×10^{-3}	1.0×10^{-4}	[53]
Smartphone coupled µPAD	1.0×10^{-4}–1.0×10^{-2}	4.7×10^{-5}	[54]
Polybithiophene-palladium particle	4.0×10^{-5}–4.0×10^{-4}	7.0×10^{-6}	[55]
PEDOT-Pd-GOx	5.0×10^{-4}–3.0×10^{-2}	7.5×10^{-5}	[56]
MIP/TNO@NC/GCE	***1.0×10^{-5}–5.0×10^{-3}***	***1.0×10^{-6}***	***This study***

CuO/ITO copper(II) oxide/indium tin oxide, *rGO/APBA* reduced graphene oxide/3-amino phenylboronic acid, *APBA/GNPs* 3-amino phenylboronic acid/gold nanoantennas, *CNTs/PBA* phenylboronic acid functionalized carbon nanotubes, *SERS* surface-enhanced Raman spectroscopy, *µPAD* paper-based microfluidic devices, *PEDOT-Pd-GOx* poly(3,4-ethylenedioxythiophene)-palladium nanoparticles-glucose oxidase

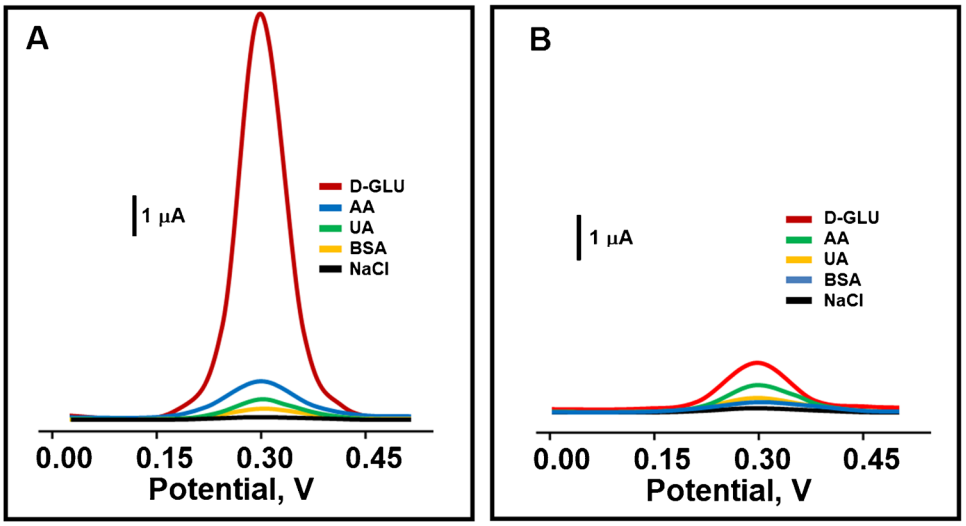

Fig. 7 Differential pulse voltammograms of **A** MIP/TNO@NC/GCE and **B** NIP/TNO@NC/GCE in 0.500 mM D-GLU, 100.0 mM AA, 100.0 mM UA, 100.0 mM BSA, and 100.0 mM NaCl (parameters are frequency of 100 Hz, pulse amplitude of 25 mV, and scan increment of 5 mV)

Table 2 k and k' values of D-GLU-imprinted electrode ($n=6$)

	MIP		NIP		
	ΔI	k	ΔI	k	k'
D-GLU	10.00 ± 0.001	-	1.000 ± 0.001	-	-
AA	1.000 ± 0.002	10.00	0.500 ± 0.002	2.00	5.00
UA	0.500 ± 0.002	20.00	0.250 ± 0.003	4.00	5.00
BSA	0.250 ± 0.001	40.00	0.200 ± 0.002	5.00	8.00
NaCl	0.100 ± 0.002	100.00	0.100 ± 0.001	10.00	10.00

k the calculated selectivity coefficient, k' relative selectivity coefficient.

Analyte concentrations: 0.500 mM D-GLU, 100.0 mM AA, 100.0 mM UA, 100.0 mM BSA, and 100.0 mM NaCl

repeated signals (approximately 10.0 A with 0.21% relative standard deviation) were detected in Fig. S5A, indicating satisfactory glucose determination stability.

In addition, the reusability of MIP/TNO@NC/GCE was examined after 50 times usage. As can be seen Fig. S5B, the stable electrochemical responses with 0.39% of RSD were observed, confirming the high reusability of D-GLU-imprinted electrochemical biosensor.

Finally, 15 D-GLU-imprinted electrochemical biosensors were separately prepared and tested in the presence of 0.500 mM D-GLU for the reproducibility test. Electrochemical signals with 0.61% of RSD at + 0.30 V verified the reliability of sensor preparation procedure.

Precision and accuracy

The studies of same day (intra-day precision) and 6 consecutive days (inter-day precision) were carried out in the presence of three concentrations (2.000, 3.000, and 4.000 mM D-GLU) in linearity range (Table S4). The values of RSD for intra-day and inter-day precision were obtained as 0.025–0.082 and 0.012–0.082, respectively. Hence, low RSD verified high precision of the prepared imprinted biosensor. Accuracy as Bias % was also tested and low Bias % (Table S4) suggested the high accuracy of the prepared imprinted biosensor.

Conclusions

In this study, the molecularly imprinting electrochemical biosensor based on a hierarchical N-rich carbon conductive-coated TNO structure was used for glucose detection in plasma samples. The preparation of N-rich carbon conductive-coated TNO structure was accomplished with minimal waste generation, providing the development of environmentally and human-friendly biosensor. A validated electrochemical method was proposed in terms of selectivity, stability, reusability, and reproducibility. Thus, glucose detection was carried out in lower concentrations by this biosensor. Hence, it is an encouraging approach for the design and application of non-enzymatic glucose sensors in practical applications.

Supplementary Information The online version contains supplementary material available at https://doi.org/10.1007/s00604-021-05128-x.

Acknowledgements Mehmet Lütfi Yola would like to thank Turkish Academy of Sciences for their invaluable support in respect to Young Scientists Award Program, TÜBA-GEBIP (2019).

Declarations

Conflict of interest The authors declare no competing interests.

References

1. Ensafi AA, Mirzaii F, Nasr-Esfahani P, Rezaei B (2020) Ni3S2 supported on porous ball-milled silicon, a highly selective electrochemical sensor for glucose determination. Electroanal 32(8):1707–1716
2. Lindqvist DN, Pedersen HAElig, Rasmussen LH (2018) A novel technique for determination of the fructose, glucose and sucrose distribution in nectar from orchids by HPLC-ELSD. J Chromatogr B. 1081:130–134
3. Liu S, Tian JQ, Wang L, Luo YL, Sun XP (2012) A general strategy for the production of photoluminescent carbon nitride dots from organic amines and their application as novel peroxidase-like catalysts for colorimetric detection of H2O2 and glucose. Rsc Adv 2(2):411–413
4. Xie WQ, Gong YX, Yu KX (2017) Rapid quantitative detection of glucose content in glucose injection by reaction headspace gas chromatography. J Chromatogr A 1520:143–146
5. Larsen T (2015) Fluorometric determination of free glucose and glucose 6-phosphate in cows' milk and other opaque matrices. Food Chem 166:283–286
6. Shen YC, Davies AG, Linfield EH, Elsey TS, Taday PF, Arnone DD (2003) The use of Fourier-transform infrared spectroscopy for the quantitative determination of glucose concentration in whole blood. Phys Med Biol 48(13):2023–2032
7. Hamtak M, Hosseini M, Fotouhi L, Aghazadeh M (2018) A new electrochemiluminescence biosensor for the detection of glucose based on polypyrrole/polyluminol/Ni(OH)(2)-C3N4/glucose oxidase-modified graphite electrode. Anal Methods-Uk 10(47):5723–5730
8. Zargoosh K, Shamsipur M, Qandalee M, Piltan M, Moradi L (2011) Sensitive and selective determination of glucose in human serum and urine based on the peroxyoxalate chemiluminescence reaction of a new Fluorophore. Spectrochim Acta A 81(1):679–683
9. Gupta VK, Atar N, Yola ML, Eryilmaz M, Torul H, Tamer U, Boyaci IH, Ustundag Z (2013) A novel glucose biosensor platform based on Ag@AuNPs modified graphene oxide nanocomposite and SERS application. J Colloid Interf Sci 406:231–237
10. Archana V, Xia Y, Fang RY, Kumar GG (2019) Hierarchical CuO/NiO-carbon nanocomposite derived from metal organic framework on cello tape for the flexible and high performance nonenzymatic electrochemical glucose sensors. Acs Sustain Chem Eng 7(7):6707–6719
11. Xu ZH, Wang QZ, Hui ZS, Zhao S, Zhao YJ, Wang L (2021) Carbon cloth-supported nanorod-like conductive Ni/Co bimetal MOF: a stable and high-performance enzyme-free electrochemical sensor for determination of glucose in serum and beverage. Food Chem 349:129202
12. Boubezari I, Zazoua A, Errachid A, Jaffrezic-Renault N (2021) Sensitive electrochemical detection of bioactive molecules (hydrogen peroxide, glucose, dopamine) with perovskites-based sensors. Chemosensors 9(10):289
13. Boubezari I, Zazoua A, Bessueille F, Errachid A, Jaffrezic-Renault N (2020) Design of a new non-enzymatic sensor based on a substituted A(2)BO(4+delta) perovskite for the voltammetric detection of glucose. Electroanal 32(7):1642–1650
14. Atta NF, Galal A, El-Ads EH (2019) Effect of B-site doping on Sr2PdO3 perovskite catalyst activity for non-enzymatic determination of glucose in biological fluids. J Electroanal Chem. 852:113523
15 Shafi PM, Joseph N, Karthik R, Shim JJ, Bose AC, Ganesh V (2021) Lemon juice-assisted synthesis of LaMnO3 perovskite nanoparticles for electrochemical detection of dopamine. Microchem J. 164:105945
16. Yu HX, Cheng X, Zhu HJ, Zheng RT, Liu TT, Zhang JD, Shui M, Xie Y, Shu J (2018) Deep insights into kinetics and structural evolution of nitrogen-doped carbon coated TiNb24O62 nanowires as high-performance lithium container. Nano Energy 54:227–237
17. Lou SF, Cheng XQ, Gao JL, Li Q, Wang L, Cao Y, Ma YL, Zuo PJ, Gao YZ, Du CY, Huo H, Yin GP (2018) Pseudocapacitive Li+ intercalation in porous Ti2Nb10O29 nanospheres enables ultrafast lithium storage. Energy Storage Mater 11:57–66
18. Xing LD, Yu QY, Jiang B, Chu JH, Lao CY, Wang M, Han K, Liu ZW, Bao YP, Wang W (2019) Carbon-encapsulated ultrathin MoS2 nanosheets epitaxially grown on porous metallic TiNb2O6 microspheres with unsaturated oxygen atoms for superior potassium storage. J Mater Chem A 7(10):5760–5768
19. Mao WT, Liu KC, Guo G, Liu GY, Bao KY, Guo JL, Hu M, Wang WB, Li BB, Zhang KL, Qian YT (2017) Preparation and electrochemical performance of Ti2Nb10O29/Ag composite as anode materials for lithium ion batteries. Electrochim Acta 253:396–402
20. Griffith KJ, Forse AC, Griffin JM, Grey CP (2016) High-rate intercalation without nanostructuring in metastable Nb2O5 bronze phases. J Am Chem Soc 138(28):8888–8899
21. Griffith KJ, Senyshyn A, Grey CP (2017) Structural stability from crystallographic shear in TiO2-Nb2O5 phases: cation ordering and lithiation behavior of TiNb24O62. Inorg Chem 56(7):4002–4010
22. Wang XF, Shen GZ (2015) Intercalation pseudo-capacitive TiNb2O7 carbon electrode for high-performance lithium ion hybrid electrochemical supercapacitors with ultrahigh energy density. Nano Energy 15:104–115
23. Fei L, Xu Y, Wu X, Li Y, Xie P, Deng S, Smirnov S, Luo H (2013) SBA-15 confined synthesis of TiNb2O7 nanoparticles for lithium-ion batteries. Nanoscale 5(22):11102–11107
24. Cheng QS, Liang JW, Zhu YC, Si LL, Guo C, Qian YT (2014) Bulk Ti2Nb10O29 as long-life and high-power Li-ion battery anodes. J Mater Chem A 2(41):17258–17262
25. Yuan T, Luo SN, Soule L, Wang JH, Wang YC, Sun DW, Zhao B, Li WW, Yang JH, Zheng SY, Lin ML (2020) A hierarchical Ti2Nb10O29 composite electrode for high-power lithium-ion batteries and capacitors. Mater Today 45:8–19
26. Akyildirim O, Kardas F, Beytur M, Yuksek H, Atar N, Yola ML (2017) Palladium nanoparticles functionalized graphene quantum dots with molecularly imprinted polymer for electrochemical analysis of citrinin. J Mol Liq 243:677–681
27. Beytur M, Kardas F, Akyildirim O, Ozkan A, Bankoglu B, Yuksek H, Yola ML, Atar N (2018) A highly selective and sensitive voltammetric sensor with molecularly imprinted polymer based silver@gold nanoparticles/ionic liquid modified glassy carbon electrode for determination of ceftizoxime. J Mol Liq 251:212–217
28. Spivak DA (2006) Optimization, evaluation, and characterization of molecularly imprinted polymers (vol 57, pg 1779, 2005). Adv Drug Deliver Rev 58(1):116
29. Ozcan N, Karaman C, Atar N, Karaman O, Yola ML (2020) A novel molecularly imprinting biosensor including graphene quantum dots/multi-walled carbon nanotubes composite for interleukin-6 detection and electrochemical biosensor validation. Ecs J Solid State Sc. 9(12):121010
30. Ozcan N, Medetalibeyoglu H, Akyildirim O, Atar N, Yola ML (2020) Electrochemical detection of amyloid-beta protein by delaminated titanium carbide MXene/multi-walled carbon nanotubes composite with molecularly imprinted polymer. Mater Today Commun. 23:101097
31. Mohammadi A, Hasan MA, Liedberg B, Lundstrom I, Salaneck WR (1986) Chemical vapor-deposition (Cvd) of conducting polymers - polypyrrole. Synthetic Met 14(3):189–197
32. Yola ML, Atar N, Qureshi MS, Ustundag Z, Solak AO (2012) Electrochemically grafted etodolac film on glassy carbon for Pb(II) determination. Sensor Actuat B-Chem 171:1207–1215

33. Yola ML, Atar N (2019) Development of cardiac troponin-I biosensor based on boron nitride quantum dots including molecularly imprinted polymer. Biosens Bioelectron 126:418–424
34. Griffith KJ, Wiaderek KM, Cibin G, Marbella LE, Grey CP (2018) Niobium tungsten oxides for high-rate lithium-ion energy storage. Nature 559(7715):556–563
35. Zhang XY, Deng SJ, Zeng YX, Yu MH, Zhong Y, Xia XH, Tong YX, Lu XH (2018) Oxygen defect modulated titanium niobium oxide on graphene arrays: an open-door for high-performance 1.4 V symmetric supercapacitor in acidic aqueous electrolyte. Adv Funct Mater. 28(44):1805618
36. Luo SN, Zhang PC, Yuan T, Ruan JF, Peng CX, Pang YP, Sun H, Yang JH, Zheng SY (2018) Molecular self-assembly of a nanorod N-Li4Ti5O12/TiO2/C anode for superior lithium ion storage. J Mater Chem A 6(32):15755–15761
37. Yuan T, He YS, Zhang WM, Ma ZF (2016) A nitrogen-containing carbon film derived from vapor phase polymerized polypyrrole as a fast charging/discharging capability anode for lithium-ion batteries. Chem Commun 52(1):112–115
38. Deng SJ, Luo ZB, Liu YT, Lou XM, Lin CF, Yang C, Zhao H, Zheng P, Sun ZL, Li JB, Wang N, Wu H (2017) Ti2Nb10O29-x mesoporous microspheres as promising anode materials for high-performance lithium-ion batteries. J Power Sources 362:250–257
39. Orliukas AF, Fung KZ, Venckute V, Kazlauskiene V, Miskinis J, Lelis M (2015) Structure, surface and broadband impedance spectroscopy of Li4Ti5O12 based ceramics with Nb and Ta. Solid State Ionics 271:34–41
40. Atashbar MZ, Sun HT, Gong B, Wlodarski W, Lamb R (1998) XPS study of Nb-doped oxygen sensing TiO2 thin films prepared by sol-gel method. Thin Solid Films 326(1–2):238–244
41. Xu ZC, Li Q, Gao SA, Shang JK (2012) Synthesis and characterization of niobium-doped TiO2 Nanotube arrays by anodization of Ti-20Nb alloys. J Mater Sci Technol 28(10):865–870
42. Lu JJ, Ma JQ, Yi JM, Shen ZL, Zhong YJ, Ma CA, Li MC (2014) Electrochemical polymerization of pyrrole containing TEMPO side chain on Pt electrode and its electrochemical activity. Electrochim Acta 130:412–417
43. Adhami T, Ebrahimi-Kahrizsangi R, Bakhsheshi-Rad HR, Majidi S, Ghorbanzadeh M, Berto F (2021) Synthesis and electrochemical properties of TiNb2O7 and Ti2Nb10O29 anodes under various annealing atmospheres. Metals-Basel 11(6):983
44. Yang J, Hu Y, Li YC (2019) Molecularly imprinted polymer-decorated signal on-off ratiometric electrochemical sensor for selective and robust dopamine detection. Biosens Bioelectron 135:224–230
45. Karimi-Maleh H, Yola ML, Atar N, Orooji Y, Karimi F, Kumar PS, Rouhi J, Baghayeri M (2021) A novel detection method for organophosphorus insecticide fenamiphos: molecularly imprinted electrochemical sensor based on core-shell Co3O4@MOF-74 nanocomposite. J Colloid Interf Sci 592:174–185
46. Bansal N (2015) Prediabetes diagnosis and treatment: a review. World J Diabetes 6(2):296–303
47. Omer AE, Shaker G, Safavi-Naeini S, Kokabi H, Alquie G, Deshours F, Shubair RM (2020) Low-cost portable microwave sensor for non-invasive monitoring of blood glucose level: novel design utilizing a four-cell CSRR hexagonal configuration. Sci Rep-Uk 10(1):15200
48. Nacef M, Chelaghmia ML, Affoune AM, Pontie M (2019) Electrochemical Investigation of glucose on a highly sensitive nickel-copper modified pencil graphite electrode. Electroanal 31(1):113–120
49. Dung NQ, Duong TTT, Lam TD, Dung DD, Huy NN, Thanh DV (2019) A simple route for electrochemical glucose sensing using background current subtraction of cyclic voltammetry technique. J Electroanal Chem. 848:113323
50. Ji DZ, Liu L, Li S, Chen C, Lu YL, Wu JJ, Liu QJ (2017) Smartphone-based cyclic voltammetry system with graphene modified screen printed electrodes for glucose detection. Biosens Bioelectron 98:449–456
51. Mesch M, Zhang CJ, Braun PV, Giessen H (2015) Functionalized hydrogel on plasmonic nanoantennas for noninvasive glucose sensing. ACS Photonics 2(4):475–480
52. Chen GS, Qiu JL, Xu JQ, Fang XA, Liu Y, Liu SQ, Wei SB, Jiang RF, Luan TG, Zeng F, Zhu F, Ouyang GF (2016) A novel probe based on phenylboronic acid functionalized carbon nanotubes for ultrasensitive carbohydrate determination in biofluids and semi-solid biotissues. Chem Sci 7(2):1487–1495
53. Kong KV, Ho CJH, Gong TX, Lau WKO, Olivo M (2014) Sensitive SERS glucose sensing in biological media using alkyne functionalized boronic acid on planar substrates. Biosens Bioelectron 56:186–191
54. Mercan OB, Kilic V, Sen M (2021) Machine learning-based colorimetric determination of glucose in artificial saliva with different reagents using a smartphone coupled mu PAD. Sensor Actuat B-Chem. 329:129037
55. Lamiri L, Belgherbi O, Dehchar C, Laidoudi S, Tounsi A, Nessark B, Habelhames F, Hamam A, Gourari B (2020) Performance of polybithiophene-palladium particles modified electrode for non-enzymatic glucose detection. Synthetic Met. 266:116437
56. Santhosh P, Manesh KM, Uthayakumar S, Komathi S, Gopalan AI, Lee KP (2009) Fabrication of enzymatic glucose biosensor based on palladium nanoparticles dispersed onto poly(3,4-ethylenedioxythiophene) nanofibers. Bioelectrochemistry 75(1):61–66
57. Rogatsky E, Tomuta V, Stein DT (2007) LC/MS quantitative study of glucose by iodine attachment. Anal Chim Acta 591(2):155–160